

## Metallic dimers: When bonding transverse modes shine light

Brice Rolly, Brian Stout, and Nicolas Bonod\*

*Institut Fresnel, CNRS, Aix-Marseille Université, Ecole Centrale Marseille, Campus de Saint-Jérôme, F-13013 Marseille, France*

(Received 23 March 2011; revised manuscript received 5 July 2011; published 8 September 2011)

The optical properties of dimers of dipolar metallic particles of a typical size of 100 nm cannot be predicted by the quasistatic approximation, even for nanogap sizes much smaller than the wavelength of the illuminating light, due to the strong interparticle scattering. Nonquasistatic expressions for scattering cross sections show that the transverse bonding mode becomes the brightest mode for decreasing nanogaps in the antenna, and the fundamental role of the interparticle scattering term in these unexpected optical properties is demonstrated.

DOI: [10.1103/PhysRevB.84.125420](https://doi.org/10.1103/PhysRevB.84.125420)

PACS number(s): 78.67.-n, 78.40.-q, 42.25.Fx, 73.22.Lp

### I. INTRODUCTION

Nanogap antennas can serve to concentrate light into tiny volumes, thereby allowing strong interactions between light and very small amounts of matter. Metallic dimers have been investigated successfully for conceiving biosensors able to probe matter at the molecular level,<sup>1-3</sup> create optical traps for particles,<sup>4,5</sup> or serve as reproducible Raman spectrometers.<sup>6</sup> These applications exploit the hot spots produced in the nanogaps between neighboring particles through the coupling of individual-particle dipole modes into bonding and antibonding modes.<sup>7</sup> In the optical frequency range, the quasistatic approximation is valid for dimers of spheres roughly smaller than 50 nm in diameter with nanometric separations. In the quasistatic approximation, opposite phase modes are dark, i.e., exhibiting small scattering cross sections. Those “dark” modes have been extensively studied recently, since they can produce magnetic permeability<sup>8</sup> or control the quantum yield of an emitter.<sup>9</sup> Experiments typically employ somewhat larger particles,  $\sim 100$  nm in diameter, for technological reasons but also because their larger scattering cross sections facilitate the probing of the scattered light.

Although the quasistatic approximation remains reasonable for isolated particles, it fails when dipolar particles are strongly coupled.<sup>10,11</sup> We show that for nanogaps as small as 25 nm, transverse bonding modes that are expected to be dark from a quasistatic standpoint can actually behave as bright modes (and vice versa). In this work, we develop nonquasistatic expressions for the scattering cross sections of metallic dimers, which explain and predict these features. The behavior of the interparticle scattering field is a key issue in this study, and its phase dependence with respect to the nanogap length will be investigated thoroughly. Our conclusions and results are verified by a full electromagnetic treatment implemented in the framework of the generalized Mie theory.<sup>12</sup>

This paper is organized as follows: In Sec. II, we show that for a certain configuration, the transverse bonding mode of a dimer can be “bright,” i.e., it can present a large scattering cross section. In Sec. III, we develop a nonquasistatic dipolar model that is able to reproduce accurately this behavior, and we reveal the crucial role played by the interparticle scattering field. We conclude in Sec. IV.

### II. A BRIGHT TRANSVERSE BONDING MODE

#### A. Conditions of illumination

We consider a dimer of silver spherical particles (diameters  $D = 110$  nm, permittivity extrapolated from experimental values of Palik and Ghosh<sup>13</sup>) in a polymer environment of refractive index  $n_m = 1.5$ , where the two spherical scatterers have a center-to-center separation  $d$ , and are placed along either the  $\hat{x}$  axis or the  $\hat{z}$  axis, depending on the studied illumination conditions (see Fig. 1). The different particle orientations were chosen so that the incident electric field can be conveniently taken to lie along the  $\hat{z}$  axis throughout this study, i.e.,

$$\begin{aligned} \mathbf{E}_{\text{inc},L}(x) &= \mathbf{E}_{\text{inc},T,k_{\parallel}}(x) = E_0 \hat{z} e^{ikx}, \\ \mathbf{E}_{\text{inc},T,k_{\perp}}(y) &= E_0 \hat{z} e^{iky}, \end{aligned} \quad (1)$$

where  $k = (\omega/c)n_m$  is the wave number of the incoming plane wave in the embedding polymer. The induced dipole moments of each particle are also aligned along the  $\hat{z}$  axis, and can be expressed as

$$\mathbf{p}^{(j)}(\omega) = \epsilon_0 \epsilon_m \alpha(\omega) E_{\text{exc}}^{(j)}(\omega) \hat{z}, \quad (2)$$

where  $j$  is the particle label and  $E_{\text{exc}}^{(j)}$  is the exciting electric field associated with the particle. In this work, the dipolar polarizability,  $\alpha$ , is extracted from the electric dipole Mie coefficient,<sup>14,15</sup>  $a_1$ , via the relation<sup>12</sup>  $\alpha = 6\pi a_1 / ik^3$ , thus avoiding the quasistatic approximation (we use a polarizability that is  $4\pi$  times the one in the above-mentioned work by Doyle). This formulation automatically includes the so-called radiation damping effects and more generally all the absorption effects, which, in “pointlike scatterer” models, have to be included as corrections.

#### B. Results

The generalized Mie theory is implemented to accurately calculate both the scattering cross section and the electric field at the center of each metallic particle. We plot the relative phase of the two induced dipoles as a function of the incident wavelength together with the scattering cross section of the dimer (Fig. 2). In this paper, we focus on wavelengths between 500 and 750 nm, where all dipolar phenomena occur for the studied dimer. Hence the features of the cross sections around

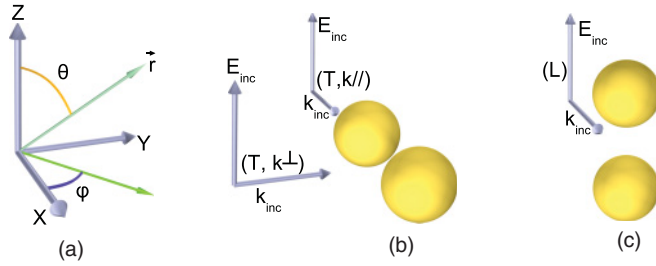


FIG. 1. (Color online) (a) Definition of the spherical coordinates; dimer illumination schematics for (b) transverse illuminations and (c) longitudinal illumination.

$\lambda = 425$  nm, which are of a multipolar nature (quadrupolar for the most part), will not be described.

Symmetry dictates identical phases for the induced dipoles of a dimer in both longitudinal and transverse  $k_{\perp}$  illuminations, but phase differences are important for a  $k_{\parallel}$  illumination. It is worth remarking that for an illumination along the dimer axis (i.e.,  $T, k_{\parallel}$ ) and nanogaps much smaller than the incident wavelength (like both the 25 and 100 nm cases), the maximum of the scattering cross section does not correspond to in-phase dipoles, but rather to strongly dephased ones. In the case of a 100 nm nanogap [Fig. 2(b)], the two induced dipoles are in fully opposite phase at the scattering cross-section maximum. Moreover, the nearly opposite phase mode observed for the 25 nm nanogap has a larger scattering efficiency than the in-phase mode observed for an illumination perpendicular to the dimer axis,  $k_{\perp}$ . Let us emphasize that this study is performed on particles having diameters near those investigated experimentally<sup>16–20</sup> separated by tiny nanogaps (e.g., 25 nm in Fig. 2, left). It is thus of fundamental importance to reveal the physical properties responsible for such unexpected properties. To this end, we derive below an analytical formalism able to accurately predict the scattering efficiency maxima of metallic dimers in terms of particle polarizabilities and separations.

### III. EFFECTIVE POLARIZABILITY MODEL

#### A. Derivation

Let us now develop an effective polarizability approach<sup>21–24</sup> wherein the multiple scattering phenomena occurring between

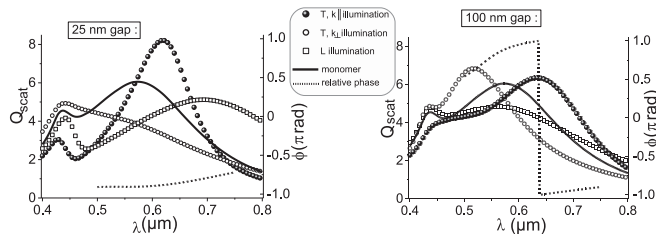


FIG. 2. Silver particles,  $D = 110$  nm in diameter, with respective nanogap sizes,  $(d - D)$ , of 25 nm (left) and 100 nm (right). Full lines and symbols, left scale: Scattering efficiencies *per particle*,  $Q_{\text{scat}} \equiv \sigma_{\text{scat}}/(2\pi a^2)$ ; full circles:  $T, k_{\parallel}$  and (open circles)  $T, k_{\perp}$  illuminations; open squares:  $L$  illumination; full lines: values for the monomer  $[\sigma_{\text{scat}}/(\pi a^2)]$ . Dashed black line, right scale: Relative phase of the induced dipoles for the  $T, k_{\parallel}$  illumination.

the two spheres are assimilated into an “effective” polarizability (which depends on the incident illumination orientation and polarization). The electric field produced by an electric dipole moment  $\mathbf{p}^{(j)}$  can be expressed as<sup>25</sup>

$$\mathbf{E}_{\text{scat}}^{(j)}(\mathbf{r}) = \frac{e^{ikr}}{4\pi\epsilon_m\epsilon_0 r^3} \{k^2 r^2 (\hat{\mathbf{r}} \times \mathbf{p}^{(j)}) \times \hat{\mathbf{r}} + (1 - ikr)[3(\hat{\mathbf{r}} \cdot \mathbf{p}^{(j)})\hat{\mathbf{r}} - \mathbf{p}^{(j)}]\}. \quad (3)$$

For an incident field polarized in the  $z$  direction, the excitation field at the center of a sphere  $j$ ,  $E_{\text{exc}}^{(j)}$  (in the configurations of Fig. 1), also lies along the  $\hat{\mathbf{z}}$  direction and is the sum of the incident field and the field scattered by the other sphere  $i$ :  $E_{\text{exc}}^{(j)} \equiv [\mathbf{E}_{\text{inc}}(x_j) + \mathbf{E}_{\text{scat}}^{(i)}(x_j)] \cdot \hat{\mathbf{z}}$ . The excitation fields for spheres 1 and 2 can then be written as (see Appendix A)

$$E_{\text{exc}}^{(1)} = E_{\text{inc}}^{(1)} + \gamma E_{\text{exc}}^{(2)}, \quad (4a)$$

$$E_{\text{exc}}^{(2)} = E_{\text{inc}}^{(2)} + \gamma E_{\text{exc}}^{(1)}, \quad (4b)$$

where  $\gamma$  is defined to represent the interparticle scattering couplings (either purely transverse or longitudinal for the cases studied here):

$$\gamma_T = \gamma_T^{k_{\parallel}} = \gamma_T^{k_{\perp}} \equiv e^{ikd} \frac{\alpha}{4\pi d^3} (k^2 d^2 + ikd - 1), \quad (5a)$$

$$\gamma_L \equiv e^{ikd} \frac{\alpha}{2\pi d^3} (1 - ikd). \quad (5b)$$

We remark in these expressions of  $\gamma_{L,T}$  that the propagation term,  $e^{ikd}$ , is only *partly* responsible for the phase of  $\gamma_{L,T}$ , and we can readily surmise that the respective factors  $(k^2 d^2 + ikd - 1)$  and  $(1 - ikd)$  play non-negligible roles on the phase of  $\gamma_{L,T}$ , particularly at distances that are small or comparable to the wavelength.

The solution to the system of coupled equations [Eqs. (4a) and (4b)] can be expressed in terms of “effective” polarizabilities that read (see Appendix A)

$$\alpha_{\text{eff}, T, k_{\parallel}}^{(1)} = \alpha \frac{1 + \gamma_T e^{ikd}}{1 - \gamma_T^2}, \quad (6a)$$

$$\alpha_{\text{eff}, T, k_{\parallel}}^{(2)} = \alpha \frac{1 + \gamma_T e^{-ikd}}{1 - \gamma_T^2}, \quad (6b)$$

$$\alpha_{\text{eff}, T, k_{\perp}}^{(1)} = \alpha_{\text{eff}, T, k_{\perp}}^{(2)} = \alpha \frac{1 + \gamma_T}{1 - \gamma_T^2} = \frac{\alpha}{1 - \gamma_T}, \quad (6c)$$

$$\alpha_{\text{eff}, L}^{(1)} = \alpha_{\text{eff}, L}^{(2)} = \frac{\alpha}{1 - \gamma_L}, \quad (6d)$$

which express the induced dipole moments directly in terms of the incident field, i.e.,

$$\mathbf{p}^{(j)}(\omega) = \epsilon_0 \epsilon_m \alpha_{\text{eff}}^{(j)}(\omega) E_{\text{inc}}^{(j)}(\omega) \hat{\mathbf{z}}. \quad (7)$$

The effective polarizabilities are thus proportional to the single-particle polarizability, and to a term involving the interparticle coupling  $\gamma$ . We obtain in this manner an analytical expression for the relative phase,  $\phi$ , between the two induced dipoles in the  $T, k_{\parallel}$  case,

$$\phi = \arg(p_2/p_1) = \arg\left(\frac{e^{ikd} (1 + \gamma_T e^{-ikd})}{1 + \gamma_T e^{ikd}}\right). \quad (8)$$

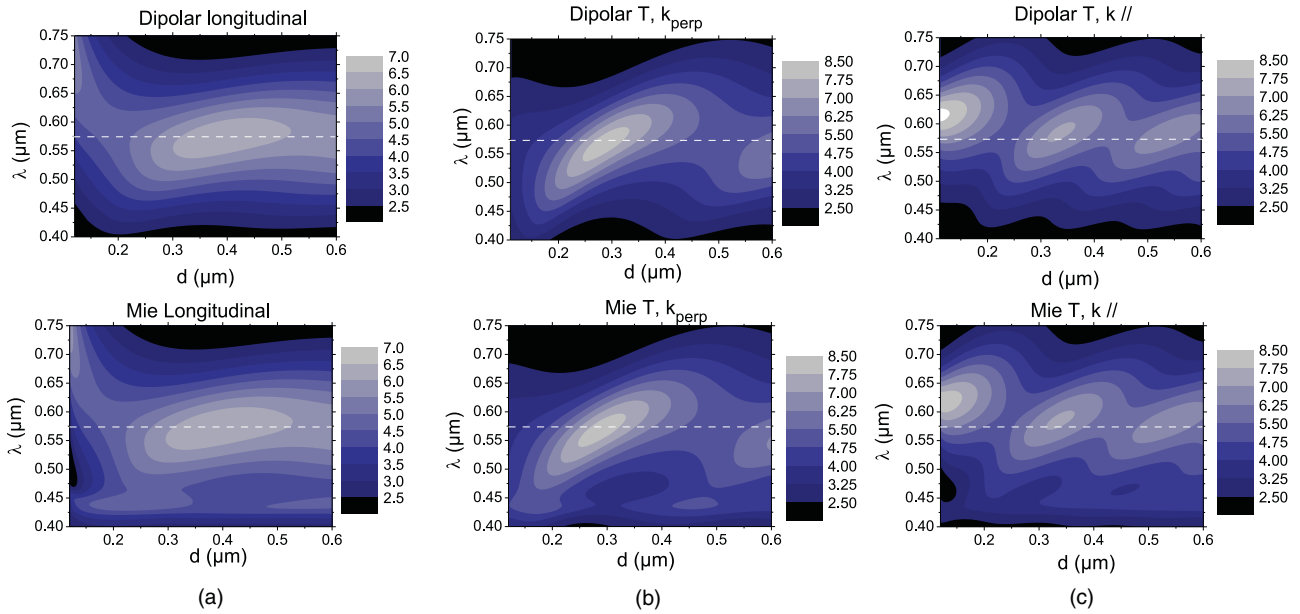


FIG. 3. (Color online) Top row: Scattering efficiency calculated with the dipolar model, vs the center-to-center separation,  $d$ , and the wavelength, for a dimer of silver spherical particles 110 nm in diameter. The center-to-center particle separation lies on the abscissa, and the vacuum wavelength on the ordinate (both in micrometers); (a) longitudinal illumination, (b)  $T, k_{\perp}$  illumination, and (c)  $T, k_{\parallel}$  illumination. The bottom row displays the same quantities using calculations from the generalized Mie theory.

We demonstrate in Appendix B that scattering cross sections of a dimer of dipolar particles are closely linked to the square modulus of the effective polarizabilities in a manner similar to the scattering efficiency of a monomer that is directly proportional to the square modulus of its polarizability. The total scattering cross section  $\sigma_{\text{scat}}$  (Ref. 12) can thus be cast,

$$\sigma_{\text{scat}, T, k_{\parallel}} = \frac{k^4}{6\pi} \left[ |\alpha_{\text{eff}, T, k_{\parallel}}^{(1)}|^2 + |\alpha_{\text{eff}, T, k_{\parallel}}^{(2)}|^2 + 2 \text{Re}[\alpha_{\text{eff}, T, k_{\parallel}}^{(1)} (\alpha_{\text{eff}, T, k_{\parallel}}^{(2)})^* e^{-ikd}] A_T \right], \quad (9a)$$

$$\sigma_{\text{scat}, T, k_{\perp}} = \frac{k^4}{3\pi} |\alpha_{\text{eff}, T, k_{\perp}}^{(1)}|^2 (1 + A_T), \quad (9b)$$

$$\sigma_{\text{scat}}^L = \frac{k^4}{3\pi} |\alpha_{\text{eff}, L}^{(1)}|^2 (1 + A_L), \quad (9c)$$

where the factors  $A_{T,L}$  are, respectively, defined to contain the radiative interference effects:

$$A_T \equiv 3 \frac{(k^2 d^2 - 1) \sin(kd) + kd \cos(kd)}{2(kd)^3}, \quad (10)$$

$$A_L \equiv 3 \frac{\sin(kd) - kd \cos(kd)}{(kd)^3}.$$

The radiative interference terms,  $A_{T,L}$ , can both be replaced by 1 in the limit of  $kd \rightarrow 0$  (third order), and decrease only slowly with increasing  $kd$ . Consequently, their  $kd$  dependence can be safely ignored during this study. For the sake of completeness, we also derive the extinction cross sections in Appendix C. In Appendix D, we show the relative error between this approximation and the quasixact generalized Mie theory that we used in this study. Finding the general applicability domain of this nonquasistatic dipolar approach

is beyond the scope of this paper, but we can state that for the studied system, the relative error in the ( $550 < \lambda < 750$  nm) region of the spectrum does not exceed 10% for separations  $d > 50$  nm, and remains in most cases under 5% for all separations.

## B. Results and discussion

The normalized per sphere scattering efficiencies,  $Q_{\text{scat}}$  (cf. Fig. 2), are plotted in Fig. 3 for all three illuminations as functions of  $\lambda$  and  $d$  using both the above analytic model and full electromagnetic calculations (generalized Mie theory with  $n_{\text{max}} = 20$  maximum multipole order). The monomer resonance frequency is indicated in all graphs by a dashed white line. One can see that the analytic dipole formalism remarkably predicts that (i) transverse couplings can produce larger scattering cross sections than longitudinal couplings, and that (ii) for in-phase dipoles modes (longitudinal and  $T, k_{\perp}$  illuminations) the maxima are not obtained when the separation is minimal ( $d - D \rightarrow 0$ ), but rather for separations of  $d = 450$  and  $300$  nm, respectively. Although the formalism we use in the present paper does not take into account any nonlocal permittivity effect, nor the behavior of the spheres in the conductive contact limit,<sup>26,27</sup> the calculations remain valid for small distances provided we use a high enough multipole order to allow convergence.<sup>28</sup> We also remark on a pseudoperiodicity of the scattering efficiencies in all three considered illuminations, first observed experimentally by Olk *et al.* in 2007.<sup>29</sup> We will see below that the study of Eqs. (9a)–(9c) provides a quantitative estimate of the periodicity and explains why the periodicity in the longitudinal and  $T, k_{\perp}$  illuminations is twice as large as that observed for the  $T, k_{\parallel}$  illumination.

If we neglect the influence of the numerator in Eqs. (6a) and (6b), and define  $K_T \equiv |\gamma_T|$ ,  $K_L \equiv |\gamma_L|$ ,  $\Theta_T \equiv \arg(\gamma_T)$ , and  $\Theta_L \equiv \arg(\gamma_L)$ , we deduce from Eqs. (6a)–(6d)

$$|\alpha_{\text{eff},T,k_{\parallel}}|^2 \cong \frac{|\alpha|^2}{|1 - (K_T e^{i\Theta_T})^2|^2} = \frac{|\alpha|^2}{1 + K_T^4 - 2K_T^2 \cos(2\Theta_T)}, \quad (11a)$$

$$|\alpha_{\text{eff},T,k_{\perp}}|^2 = \frac{|\alpha|^2}{|1 - K_T e^{i\Theta_T}|^2} = \frac{|\alpha|^2}{1 + K_T^2 - 2K_T \cos \Theta_T}, \quad (11b)$$

$$|\alpha_{\text{eff},L}|^2 = \frac{|\alpha|^2}{|1 - K_L e^{i\Theta_L}|^2} = \frac{|\alpha|^2}{1 + K_L^2 - 2K_L \cos \Theta_L}. \quad (11c)$$

Let us now show that this set of equations can predict which nanogap separations and wavelengths produce scattering efficiencies maxima. We begin by casting the “resonant” values,  $\Theta_R$ , of the coupling phase [i.e., those that minimize the respective denominators in Eqs. (11a)–(11c)]:

$$\Theta_{R,T,k_{\parallel}} = 0[2\pi] \text{ or } \pi[2\pi], \quad (12a)$$

$$\Theta_{R,T,k_{\perp}} = 0[2\pi], \quad (12b)$$

$$\Theta_{R,L} = 0[2\pi]. \quad (12c)$$

The argument of  $\gamma$ ,  $\Theta$ , corresponds to the argument of the sphere’s polarizability ( $\arg \alpha$ ), plus the argument of the interparticle scattering (e.g.,  $\arg[e^{ikd}(k^2d^2 + ikd - 1)]$  for transverse couplings). Equation (12) implies that when the dimer is illuminated perpendicularly to its axis [Eqs. (12b) and (12c)], the scattering from one sphere to the other must result in a dephasing of  $2\pi$ , while when the dimer is illuminated along its axis [Eq. (12a)], it can be either equal to  $\pi$  or to  $2\pi$ . Hence, the round trip of the scattered light (from one sphere to the other, and back to the first one, for a total dephasing of  $2\Theta$ ) must be constructive ( $2\Theta = 0[2\pi]$ ) with the field of the first sphere; for illuminations perpendicular to the dimer axis, there is an additional condition in that the coupling from one sphere to the other is not destructive ( $\Theta \neq \pi$ ) because they have the same excitation field by symmetry arguments. This is why the  $T,k_{\parallel}$  illumination has two possible phases, 0 or  $\pi$ , for  $\Theta$  [Eq. (12a)] while the other configurations have only one possibility for a resonant coupling,  $\Theta = 0$  [Eqs. (12b) and (12c)]. The effect of the interparticle scattering term has been largely neglected in previous works since the involved distances are much smaller than the incident wavelength but the terms  $k^2d^2 + ikd - 1$  and  $1 - ikd$  in Eqs. (5a) and (5b) will be seen to be of fundamental importance. From Eqs. (5a) and (5b), the argument (phase) of the polarizability of the particles can be expressed as

$$\arg(\alpha) = \Theta_T - kd - \arg(k^2d^2 + ikd - 1), \quad (13a)$$

$$\arg(\alpha) = \Theta_L - kd - \arg(1 - ikd). \quad (13b)$$

As we see in Eq. (11), the effective polarizabilities, which are directly linked to the scattering efficiencies, are proportional to both the polarizability of the monomer  $\alpha$  and to a denominator whose resonance conditions are given in Eq. (12). For a passive particle (the material is not a gain medium), the possible values of the argument of the

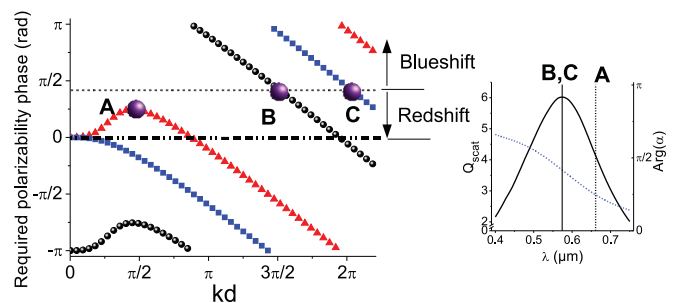


FIG. 4. (Color online) Left: Phase of the polarizability fulfilling the respective coupled resonance conditions:  $T,k_{\parallel}$  illumination (red triangles),  $T,k_{\perp}$  or  $T,k_{\parallel}$  illuminations (black circles), and longitudinal illumination (blue squares). Right inset: Scattering efficiency (solid black line, left scale) and phase of the polarizability (dashed blue line, right scale) of a  $2a = 110$  nm silver sphere embedded in a dielectric medium of refractive index  $n_m = 1.5$ . Vertical lines are plotted for a phase equal to that of point A (dashed line) and points B and C (full line) in the left figure.

polarizability lie between 0 and  $\pi$  ( $\alpha$  has a positive imaginary part). The resonance of the polarizability of the monomer under study (see the inset in Fig. 4) occurs at a vacuum wavelength  $\lambda_0 = 575$  nm, and at this wavelength the argument of the polarizability has a value  $\approx 0.42\pi$ , close to the quasistatic predicted value of  $\pi/2$ . For wavelengths blueshifted from this resonance, the argument increases toward  $\pi$ , and reciprocally it decreases to 0 for redshifted wavelengths. There is no direct link between the resonance of the polarizability and that of the coupling. Hence, usually the resonance of the scattering efficiencies will consist in a compromise between the (monomer) polarizability resonance and the coupling resonance. To illustrate this, let us plot (Fig. 4) the evolution of  $\arg(\alpha)$  as a function of  $kd$  [using Eq. (13)] required so that  $\Theta = \Theta_R$ .

This figure is of fundamental importance for the understanding of the aforementioned results: it represents the argument that the polarizability *should* have in order to obtain a resonance of the coupling term, for a given parameter  $kd$ .

Let us first look at in-phase modes under the quasistatic approximation, i.e.,  $kd \rightarrow 0$ . We remark that the redshift of the (longitudinal) bonding mode and the blueshift of the (transverse) antibonding modes (correctly predicted by the hybridization model) are also described by the nonquasistatic model presented in this study. Maximizing the scattering couplings in the  $kd \rightarrow 0$  limit requires a polarizability phase tending toward zero for the longitudinal (bonding) mode and  $\pi$  for the transverse (antibonding) mode. While both those conditions cannot be achieved simultaneously at a resonance of the polarizability [which requires  $\arg(\alpha) \approx \pi/2$ ], a compromise between the coupling resonance and the polarizability of the monomer results in the wavelength of the resonance shifting toward red (bonding) or blue (antibonding) wavelengths, respectively, compared to the resonance of the monomer.

For the more dephased excitations obtained with a  $T,k_{\parallel}$  illumination, a study of point A in Fig. 4 shows that the coupling term can be optimized near  $kd = \sqrt{2} \approx \pi/2$ , i.e., near the contact situation (contact being described at  $\lambda \cong 615$  nm by  $kd \approx 1.68 \approx \pi/2$ ) if the polarizability phase is

$\approx \pi/4$  (which implies a redshift compared to the monomer resonance). From the inset, we can see that the polarizability amplitude at this phase remains non-negligible. As predicted, we do indeed remark in Fig. 3 a redshifted resonance under the  $T, k_{\parallel}$  illumination. In general, the scattering efficiency of the  $T, k_{\parallel}$  configuration is expected to produce local maxima when either the black or red curves in Fig. 4 pass through the dotted line because the polarizability and the coupling are thus simultaneously optimized. Counting the point **A** as the first local maxima, we can see that this condition is satisfied with a period of approximately  $\pi$  respective to  $kd$ , which explains the  $\lambda/2$  periodicity of the scattering efficiency maxima in Fig. 3.

Similar considerations also predict that the  $T, k_{\perp}$  and longitudinal illuminations will be brightest around  $kd \approx 3\pi/2$  and  $kd \approx 2\pi$  (points **B** and **C**), respectively. In these respective cases, when  $kd$  increases, the required  $\arg(\alpha)$  for a resonant coupling will vary from  $\pi$  to 0, inducing blue then redshifts of the scattering efficiency maximum when  $kd$  increases around its optimum value. Let us recall that the coupling term is rapidly decreasing with respect to  $d$  [see Eqs. (5a) and (5b)] so that its influence on the wavelength of the scattering efficiency maximum will be small when compared to the resonant polarizability of the particles. The values we obtained in Fig. 3 ( $\lambda \cong 569$  nm,  $d \cong 290$  nm, i.e.,  $kd \cong 1.53\pi$  for the  $T, k_{\perp}$  illumination, and  $\lambda \cong 571$  nm,  $d \cong 387$  nm, i.e.,  $kd \cong 2.03\pi$  for the  $L$  illumination) agree with these predictions. The dimer illuminated upon the  $T, k_{\perp}$  and longitudinal illuminations will be brightest when black and blue lines, respectively, cross the  $0.42\pi$  ordinate, explaining the twice larger periodicity of the scattering efficiency observed in Figs. 3(a) and 3(b) than that observed in Fig. 3(c) for the  $T, k_{\parallel}$  illumination.

#### IV. CONCLUSION

This study highlights the optical properties of nanogap antennas involving strongly scattering dipolar particles. In particular, we showed that the maximum scattering efficiency for nearly touching spheres occurs when the dimer is illuminated along its axis. This bright mode corresponds to strongly dephased dipoles. This bonding transverse mode, which is dark in the quasistatic approximation, is rendered “bright” by the interparticle scattering term, which plays a crucial role even with tiny nanogaps. A study of its phase allowed us to fully predict these optical properties.

#### ACKNOWLEDGMENTS

The authors would like to thank Sébastien Bidault for his interest and pertinent comments.

#### APPENDIX A: EFFECTIVE POLARIZABILITIES

Using Eq. (3), the field scattered by the sphere  $j = 1, 2$  at the center of the sphere  $i = 2, 1$  is

$$\mathbf{E}_{\text{scat}}^{(j)}(\mathbf{r}_i) = \frac{e^{ikd}}{4\pi\epsilon_m\epsilon_0d^3} \{k^2d^2(\hat{\mathbf{r}}_i \times \mathbf{p}^{(j)}) \times \hat{\mathbf{r}}_i + (1 - ikd)[3(\hat{\mathbf{r}}_i \cdot \mathbf{p}^{(j)})\hat{\mathbf{r}}_i - \mathbf{p}^{(j)}]\},$$

where  $\hat{\mathbf{r}}_i$  is the unit vector pointing from sphere  $j$  to sphere  $i$ . In the transverse case,  $\hat{\mathbf{r}}_i \cdot \mathbf{p} = 0$  and  $(\hat{\mathbf{r}}_i \times \mathbf{p}) \times \hat{\mathbf{r}}_i = \mathbf{p}$ , whereas

in the longitudinal case,  $\hat{\mathbf{r}}_i \cdot \mathbf{p} = p$  and  $\hat{\mathbf{r}}_i \times \mathbf{p} = \mathbf{0}$  (hence there is no “far field,” i.e.,  $\propto k^2d^2$  term in the longitudinal case), and we have

$$\mathbf{E}_{\text{scat},T}^{(j)}(\mathbf{r}_i) = \frac{e^{ikd}}{4\pi\epsilon_m\epsilon_0d^3}(1 - ikd + k^2d^2)\mathbf{p}^{(j)},$$

$$\mathbf{E}_{\text{scat},L}^{(j)}(\mathbf{r}_i) = \frac{e^{ikd}}{4\pi\epsilon_m\epsilon_0d^3}(ikd - 1)\mathbf{p}^{(j)}.$$

Using the notation  $\gamma$  as defined in Eqs. (5a) and (5b), we then deduce Eqs. (4a) and (4b) from the definition of the excitation fields ( $\mathbf{E}_{\text{exc}}^{(j)} \equiv [\mathbf{E}_{\text{inc}}^{(j)} + \mathbf{E}_{\text{scat}}^{(j)}] \cdot \hat{\mathbf{z}}$ ). Those coupled equations can also be written as

$$E_{\text{exc}}^{(1)} = E_{\text{inc}}^{(1)} + \gamma(E_{\text{inc}}^{(2)} + \gamma E_{\text{exc}}^{(1)}),$$

$$E_{\text{exc}}^{(1)}(1 - \gamma^2) = E_{\text{inc}}^{(1)}(1 + \gamma E_{\text{inc}}^{(2)}/E_{\text{inc}}^{(1)}),$$

$$E_{\text{exc}}^{(1)} = E_{\text{inc}}^{(1)} \frac{1 + \gamma E_{\text{inc}}^{(2)}/E_{\text{inc}}^{(1)}}{1 - \gamma^2},$$

$$E_{\text{exc}}^{(2)} = E_{\text{inc}}^{(2)} \frac{1 + \gamma E_{\text{inc}}^{(1)}/E_{\text{inc}}^{(2)}}{1 - \gamma^2}.$$

We define the “effective” polarizabilities as

$$\mathbf{p}^{(j)}(\omega) = \epsilon_0\epsilon_m\alpha(\omega)E_{\text{exc}}^{(j)}(\omega)\hat{\mathbf{z}}$$

$$= \epsilon_0\epsilon_m\alpha(\omega)E_{\text{inc}}^{(j)}\frac{E_{\text{exc}}^{(j)}}{E_{\text{inc}}^{(j)}}(\omega)\hat{\mathbf{z}}$$

$$\equiv \epsilon_0\epsilon_m\alpha_{\text{eff}}^{(j)}(\omega)E_{\text{inc}}^{(j)}(\omega)\hat{\mathbf{z}},$$

to obtain

$$\alpha_{\text{eff}}^{(j)} = \alpha \frac{1 + \gamma E_{\text{inc}}^{(i)}/E_{\text{inc}}^{(j)}}{1 - \gamma^2}, \quad (\text{A1})$$

from which we deduce Eqs. (6a)–(6d).

#### APPENDIX B: SCATTERING CROSS SECTIONS

To obtain an analytical expression of the scattering cross section, we now have to find an expression of the fields in the far-field limit. Figure 1 defines the spherical coordinate notations together with the different illuminations considered in this paper. Using

$$\hat{\mathbf{z}} = \cos(\theta)\hat{\mathbf{r}} + \sin(\theta)\hat{\theta},$$

$$|\mathbf{r} - \mathbf{x}^{(j)}| = [(x - x^{(j)})^2 + y^2 + z^2]^{1/2}$$

$$\approx (r^2 - 2xx^{(j)})^{1/2} = r \left(1 - \frac{2xx^{(j)}}{r^2}\right)^{1/2}$$

$$\approx r - x^{(j)} \sin(\theta) \cos(\phi) \equiv r - \beta_T^{(j)},$$

$$|\mathbf{r} - \mathbf{z}^{(j)}| \approx r - z^{(j)} \cos(\theta) \equiv r - \beta_L^{(j)},$$

we obtain<sup>30</sup>

$$\lim_{r \rightarrow \infty} \mathbf{E}_{\text{scat}}^{(j)}(\mathbf{r}) = (\omega/c)^2 \frac{e^{ik|\mathbf{r}-\mathbf{x}^{(j)}|}}{4\pi\epsilon_0r} (\hat{\mathbf{z}} - \hat{\mathbf{r}} \cos \theta) p^{(i)}$$

$$= (\omega/c)^2 \frac{e^{ikr} e^{-ik\beta^{(j)}}}{4\pi\epsilon_0r} (\hat{\mathbf{z}} - \hat{\mathbf{r}} \cos \theta) p^{(i)}$$

$$= (\omega/c)^2 \frac{e^{ikr} e^{-ik\beta^{(j)}}}{4\pi\epsilon_0r} p^{(i)} \sin \theta \hat{\theta},$$

which yields the total scattered electric and magnetic fields  $\mathbf{E}(\mathbf{r})$  and  $\mathbf{H}(\mathbf{r})$  in the far-field,

$$\mathbf{E}(\mathbf{r}) = (\omega/c)^2 \frac{e^{ikr}}{4\pi\epsilon_0 r} \left( \sum_{j=1}^2 p^{(j)} e^{-ik\beta^{(j)}} \right) \sin\theta \hat{\theta},$$

$$\mathbf{H}(\mathbf{r}) = \omega k \frac{e^{ikr}}{4\pi r} \left( \sum_{j=1}^2 p^{(j)} e^{-ik\beta^{(j)}} \right) \sin\theta \hat{\phi}.$$

We then have the time-averaged far-field Poynting vector  $\mathbf{P}(\mathbf{r})$ ,

$$\begin{aligned} \mathbf{P}(\mathbf{r}) &= \frac{1}{2} \text{Re}[(\mathbf{E})^* \wedge \mathbf{H}] \\ &= \frac{\sin^2(\theta)\omega^3 k}{32\pi^2 \epsilon_0 c^2 r^2} [|p^{(1)}|^2 + |p^{(2)}|^2 \\ &\quad + 2\text{Re}[p^{(1)}(p^{(2)})^* e^{ik(\beta^{(2)} - \beta^{(1)})}]] \hat{\mathbf{r}}. \end{aligned}$$

Given the incident field irradiance  $\mathbf{P}_{\text{inc}} = \frac{1}{2}|E_0|^2(\epsilon_m\epsilon_0/\mu_0)^{1/2}\hat{\mathbf{z}}$ , we can now write the differential scattering cross section (see Ref. 15 for example),

$$\begin{aligned} \frac{d^2\sigma}{d^2\Omega}(\theta, \phi) &\equiv \lim_{r \rightarrow \infty} r^2 \hat{\mathbf{r}} \cdot \frac{\mathbf{P}(\mathbf{r})}{|\mathbf{P}_{\text{inc}}|} \\ &= \frac{k^4}{16\pi^2 E_0^2} \sin^2\theta \{ |\alpha_{\text{eff}}^{(1)} E_{\text{inc}}^{(1)}|^2 + |\alpha_{\text{eff}}^{(2)} E_{\text{inc}}^{(2)}|^2 \\ &\quad + 2\text{Re}[\alpha_{\text{eff}}^{(1)} E_{\text{inc}}^{(1)} (\alpha_{\text{eff}}^{(2)} E_{\text{inc}}^{(2)})^* e^{ik(\beta^{(2)} - \beta^{(1)})}] \}, \end{aligned}$$

$$\begin{aligned} \sigma_{\text{scat}} &= \int \frac{d^2\sigma}{d^2\Omega}(\theta, \phi) d\Omega \\ &= \int \int_S \frac{d^2\sigma}{d^2\Omega}(\theta, \phi) \sin\theta d\theta d\phi \\ &= \frac{k^4}{16\pi^2 E_0^2} \left[ 2\pi (|\alpha_{\text{eff}}^{(1)} E_{\text{inc}}^{(1)}|^2 + |\alpha_{\text{eff}}^{(2)} E_{\text{inc}}^{(2)}|^2) \right. \\ &\quad \times \int_0^\pi \sin^3\theta d\theta + 2 \int \int_S \sin^3\theta d\theta d\phi \\ &\quad \left. \times \text{Re}[\alpha_{\text{eff}}^{(1)} E_{\text{inc}}^{(1)} (\alpha_{\text{eff}}^{(2)} E_{\text{inc}}^{(2)})^* e^{ik(\beta^{(2)} - \beta^{(1)})}] \right], \end{aligned}$$

where  $S$  denotes the solid angle space ( $\theta \in [0, \pi]$ ,  $\phi \in [0, 2\pi]$ ).

Let us consider the term

$$B = \int \int_S \sin^3\theta \text{Re}[\alpha_{\text{eff}}^{(1)} E_{\text{inc}}^{(1)} (\alpha_{\text{eff}}^{(2)} E_{\text{inc}}^{(2)})^* e^{ik(\beta^{(2)} - \beta^{(1)})}] d\theta d\phi.$$

At this point, we must calculate separately the  $B$  term for the three different illuminations. We first derive the  $T, k_{\parallel}$  term,

$$\begin{aligned} B_{T, k_{\parallel}} &= \int \int_S \sin^3\theta \text{Re}[\alpha_{\text{eff}, T, k_{\parallel}}^{(1)} E_0^2 e^{-ikd} (\alpha_{\text{eff}, T, k_{\parallel}}^{(2)})^* \\ &\quad \times e^{ikd \sin\theta \cos\phi}] d\theta d\phi \\ &= E_0^2 \int_0^\pi \sin^3\theta \text{Re}[\alpha_{\text{eff}, T, k_{\parallel}}^{(1)} e^{-ikd} (\alpha_{\text{eff}, T, k_{\parallel}}^{(2)})^* \\ &\quad \times \int_0^{2\pi} e^{ikd \sin\theta \cos\phi} d\phi] d\theta. \end{aligned}$$

Here we use the ordinary regular Bessel function of zeroth order  $J_0$  and the fact that it is an even function:

$$J_0(x) = J_0(-x) = \frac{1}{2\pi} \int_0^{2\pi} e^{ix \cos\phi} d\phi,$$

$$\begin{aligned} B_{T, k_{\parallel}} &= 2\pi E_0^2 \int_0^\pi \sin^3\theta \text{Re}[\alpha_{\text{eff}, T, k_{\parallel}}^{(1)} e^{-ikd} (\alpha_{\text{eff}, T, k_{\parallel}}^{(2)})^* \\ &\quad \times J_0(kd \sin\theta)] d\theta \\ &= 4\pi E_0^2 \text{Re}[\alpha_{\text{eff}, T, k_{\parallel}}^{(1)} e^{-ikd} (\alpha_{\text{eff}, T, k_{\parallel}}^{(2)})^*] \\ &\quad \times \int_0^{\pi/2} \sin^3\theta J_0(kd \sin\theta) d\theta. \end{aligned}$$

Despite our efforts, we did not find the above integral calculated “as is” in the literature. We thus used a handbook formula from Ref. 31, equation 11.4.10,

$$\int_0^{\pi/2} J_\mu(z \sin t) \sin^{\mu+1} t \cos^{2\nu+1} t dt = \frac{2^\nu \Gamma(\nu+1)}{z^{\nu+1}} J_{\mu+\nu+1}(z),$$

which is correct as long as  $\text{Re}(\mu) > -1$  and  $\text{Re}(\nu) > -1$ . Using  $z = kd$ ,  $\mu = 0$  with  $\nu = -1/2$  and  $1/2$ , the formula yields

$$\begin{aligned} C &\equiv \int_0^{\pi/2} \sin^3\theta J_0(kd \sin\theta) d\theta \\ &= \int_0^{\pi/2} \sin\theta J_0(kd \sin\theta) d\theta \\ &\quad - \int_0^{\pi/2} \sin\theta \cos^2\theta J_0(kd \sin\theta) d\theta \\ &= \frac{\Gamma(1/2)}{(2kd)^{1/2}} J_{1/2}(kd) - \frac{\sqrt{2}\Gamma(3/2)}{(kd)^{3/2}} J_{3/2}(kd) \\ &= j_0(kd) - \frac{j_1(kd)}{kd}, \end{aligned}$$

where we used  $j_0$  and  $j_1$  for the spherical Bessel functions of order 0 and 1, which have analytical formulas in terms of usual functions:

$$j_0(x) = \frac{\sin x}{x},$$

$$j_1(x) = \frac{\sin x}{x^2} - \frac{\cos x}{x}.$$

We obtain

$$\begin{aligned} B_{T, k_{\parallel}} &= 4\pi E_0^2 \text{Re}[\alpha_{\text{eff}, T, k_{\parallel}}^{(1)} e^{-ikd} (\alpha_{\text{eff}, T, k_{\parallel}}^{(2)})^*] \\ &\quad \times \left[ \sin(kd) \left( \frac{1}{kd} - \frac{1}{(kd)^3} \right) + \frac{\cos(kd)}{(kd)^2} \right]. \end{aligned}$$

The calculus is identical for the  $T, k \perp$  case,

$$\begin{aligned} B_{T, k \perp} &= 4\pi E_0^2 |\alpha_{\text{eff}, T, k \perp}|^2 \\ &\quad \times \left[ \sin(kd) \left( \frac{1}{kd} - \frac{1}{(kd)^3} \right) + \frac{\cos(kd)}{(kd)^2} \right]. \end{aligned}$$

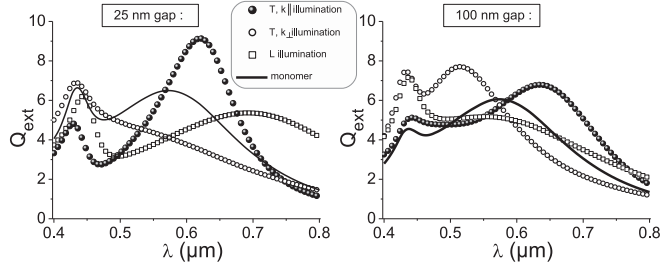


FIG. 5. Nanogap sizes ( $d - D$ ): 25 nm (left) and 100 nm (right) (see Fig. 2). Extinction efficiencies *per particle*. Full circles:  $T, k \parallel$ ; open circles:  $T, k \perp$  illuminations; open squares:  $L$  illumination; full lines: values for the monomer [ $\sigma_{\text{ext}}/(\pi a^2)$ ].

The integration of the  $B$  term for the longitudinal illumination is easier,

$$\begin{aligned}
 B_L &= \int \int_S \sin^3 \theta \operatorname{Re}[\alpha_{\text{eff},L}^{(1)} E_0^{(2)} (\alpha_{\text{eff},L}^{(2)})^* e^{ikd \cos \theta}] d\theta d\phi \\
 &= 2\pi E_0^2 |\alpha_{\text{eff},L}|^2 \int_0^\pi \sin^3 \theta \cos(kd \cos \theta) d\theta \\
 &= 2\pi E_0^2 |\alpha_{\text{eff},L}|^2 \int_{-1}^1 (1-u^2) \cos(kdu) du \\
 &= 2\pi E_0^2 |\alpha_{\text{eff},L}|^2 \left\{ -\left[ \frac{u^2}{kd} \sin(kdu) \right]_{-1}^1 \right. \\
 &\quad \left. + \int_{-1}^1 \frac{2u}{kd} \sin(kdu) du + \left[ \frac{\sin(kdu)}{kd} \right]_{-1}^1 \right\} \\
 &= 2\pi E_0^2 |\alpha_{\text{eff},L}|^2 \left\{ \left[ \frac{-2u \cos(kdu)}{(kd)^2} \right]_{-1}^1 \right. \\
 &\quad \left. - \int_{-1}^1 \frac{-2}{(kd)^2} \cos(kdu) du \right\},
 \end{aligned}$$

$$B_L = 8\pi E_0^2 |\alpha_{\text{eff},L}|^2 \left( \frac{\sin(kd)}{(kd)^3} - \frac{\cos(kd)}{(kd)^2} \right).$$

Using

$$\int_0^\pi \sin^3(\theta) d\theta = \frac{4}{3},$$

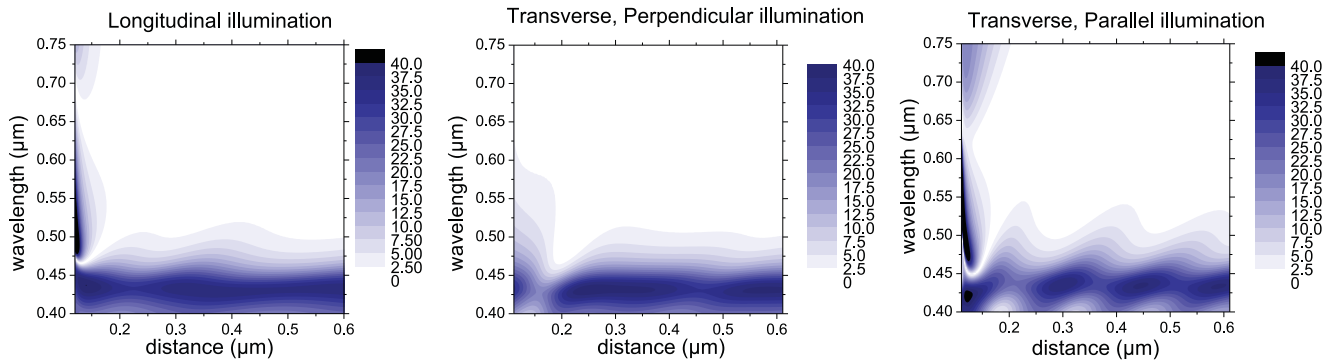


FIG. 6. (Color online) Relative error, in percentage, between the dipolar approximation and multipolar results. Left: longitudinal illumination; center:  $T, k \perp$  illumination; right:  $T, k \parallel$  illumination.

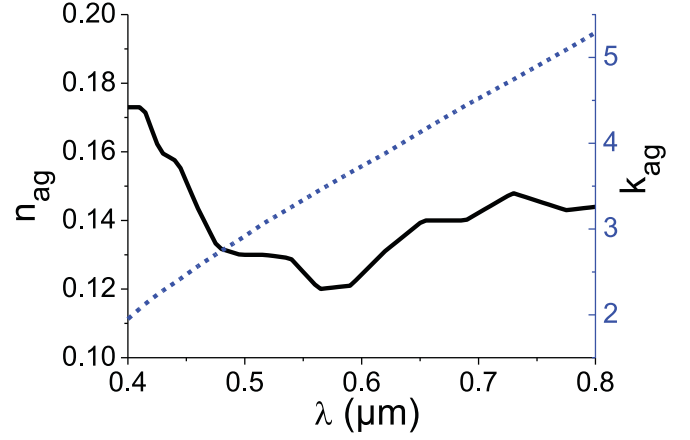


FIG. 7. (Color online) Complex refractive index of silver: real part (full black line, left scale) and imaginary part (dashed blue line, right scale).

$$\sigma_{\text{scat}} = \frac{k^4}{16\pi^2 E_0^2} \left[ 2\pi (|\alpha_{\text{eff}}^{(1)} E_{\text{inc}}^{(1)}|^2 + |\alpha_{\text{eff}}^{(2)} E_{\text{inc}}^{(2)}|^2) \frac{4}{3} + 2B \right],$$

we finally obtain

$$\begin{aligned}
 \sigma_{\text{scat},T,k\parallel} &= \frac{k^4}{6\pi} \left[ |\alpha_{\text{eff},T,k\parallel}^{(1)}|^2 + |\alpha_{\text{eff},T,k\parallel}^{(2)}|^2 \right. \\
 &\quad \left. + 2\operatorname{Re}[\alpha_{\text{eff},T,k\parallel}^{(1)} (\alpha_{\text{eff},T,k\parallel}^{(2)})^* e^{-ikd}] A^{\text{IF},T} \right], \quad (\text{B1})
 \end{aligned}$$

$$\sigma_{\text{scat},T,k\perp} = \frac{k^4}{3\pi} |\alpha_{\text{eff},T,k\perp}^{(1)}|^2 (1 + A^{\text{IF},T}), \quad (\text{B2})$$

$$\sigma_{\text{scat},L} = \frac{k^4}{3\pi} |\alpha_{\text{eff},L}^{(1)}|^2 (1 + A^{\text{IF},L}), \quad (\text{B3})$$

which are Eqs. (9a)–(9c).

### APPENDIX C: EXTINCTION CROSS SECTIONS

For the sake of completeness, we derive the formulas of the extinction cross section. With  $\tilde{\mathbf{S}}$  the scattering matrix defined by<sup>32</sup>

$$\begin{pmatrix} E_{\text{scat},\theta}(\mathbf{r}) \\ E_{\text{scat},\phi}(\mathbf{r}) \end{pmatrix} = E_0 \frac{e^{ikr}}{-ikr} \tilde{\mathbf{S}}(\mathbf{r}, \mathbf{k}_{\text{inc}}) \begin{pmatrix} E_{\text{inc},\theta} \\ E_{\text{inc},\phi} \end{pmatrix},$$

the optical theorem states that the extinction cross section  $\sigma_{\text{ext}}$  can be expressed in terms of the field scattered in the same direction as the incident field.<sup>32</sup> Specifically,

$$\sigma_{\text{ext}} = \frac{4\pi}{k^2} \text{Re}[\mathbf{e}_{\text{inc}}^* \bar{\mathbf{S}}(\hat{\mathbf{k}}_{\text{inc}}, \hat{\mathbf{k}}_{\text{inc}}) \mathbf{e}_{\text{inc}}],$$

which, in our case, yields

$$\begin{aligned} \sigma_{\text{ext},T,k\parallel} &= 2k \text{Im} \left( \alpha \frac{1 - \cos(kd)\gamma^T}{1 - (\gamma^T)^2} \right) \\ &= k \text{Im} (\alpha_{\text{eff},T,k\parallel}^{(1)} + \alpha_{\text{eff},T,k\parallel}^{(2)}), \end{aligned} \quad (\text{C1})$$

$$\sigma_{\text{ext},T,k\perp} = 2k \text{Im} \left( \frac{\alpha}{1 + \gamma^T} \right) = 2k \text{Im} (\alpha_{\text{eff},T,k\perp}^{(1)}), \quad (\text{C2})$$

$$\sigma_{\text{ext},L} = 2k \text{Im} \left( \frac{\alpha}{1 + \gamma^L} \right) = 2k \text{Im} (\alpha_{\text{eff},L}^{(1)}). \quad (\text{C3})$$

Figure 5 displays the extinction efficiencies as a function of the wavelength for the same nanogaps as in Fig. 2.

#### APPENDIX D: RELATIVE ERROR WHEN USING THE DIPOLAR MODEL

In this appendix, we present the relative error between the dipolar approximation of Eqs. (9a)–(9c) and the generalized multipolar Mie method (see Fig. 3). This error, expressed as  $\frac{|\sigma_{\text{scat,dip}} - \sigma_{\text{scat,Mie}}|}{\sigma_{\text{scat,Mie}}}$  in percentage, is presented in Fig. 6.

For all three illuminations, one can see that the error is below 2.5% in large regions. At short wavelengths ( $\lambda_0 < 550$  nm), the quadrupolar and multipolar responses of the sphere are non-negligible, hence the error becomes significant. At very small distances, the multipoles are more predominant, and the error becomes larger. However, the average error for all distances, at wavelengths  $550 < \lambda_0 < 750$  nm, is kept under 2%.

#### APPENDIX E: COMPLEX REFRACTIVE INDEX OF SILVER

Figure 7 displays the real and imaginary parts of the refractive index of silver that we use, as a function of the vacuum wavelength. Those values are based on an extrapolation from the experimental values of Palik and Ghosh.<sup>13</sup>

\*nicolas.bonod@fresnel.fr

<sup>1</sup>J. N. Anker, W. P. Hall, O. Lyandres, N. C. Shah, J. Zhao, and R. P. Van Duyne, *Nat. Mater.* **7**, 442 (2008).

<sup>2</sup>S. Lal, S. Link, and N. J. Halas, *Nat. Photon.* **1**, 641 (2007).

<sup>3</sup>S. S. Acimovic, M. P. Kreuzer, M. U. Gonzalez, and R. Quidant, *ACS Nano* **3**, 19385661 (2009).

<sup>4</sup>H. Xu and M. Käll, *Phys. Rev. Lett.* **89**, 246802 (2002).

<sup>5</sup>A. N. Grigorenko, N. W. Roberts, M. R. Dickinson, and Y. Zhang, *Nat. Photon.* **2**, 365 (2008).

<sup>6</sup>C. L. Haynes and R. P. Van Duyne, *J. Phys. Chem. B* **107**, 7426 (2003).

<sup>7</sup>P. Nordlander, C. Oubre, E. Prodan, K. Li, and M. Stockman, *Nano Lett.* **4**, 899 (2004).

<sup>8</sup>A. N. Grigorenko, A. K. Geim, H. F. Gleeson, Y. Zhang, A. A. Firsov, I. Y. Khrushchev, and J. Petrovic, *Nature (London)* **438**, 335 (2005).

<sup>9</sup>C. Vandembem, D. Brayer, L. S. Froufe-Perez, and R. Carminati, *Phys. Rev. B* **81**, 085444 (2010).

<sup>10</sup>A. F. Koenderink and A. Polman, *Phys. Rev. B* **74**, 033402 (2006).

<sup>11</sup>A. F. Koenderink, R. de Waele, J. C. Prangma, and A. Polman, *Phys. Rev. B* **76**, 201403 (2007).

<sup>12</sup>B. Stout, A. Devilez, B. Rolly, and N. Bonod, *J. Opt. Soc. Am. B* **28**, 1213 (2011).

<sup>13</sup>E. D. Palik, in *Handbook of Optical Constants of Solids* (Academic Press, New York, 1985).

<sup>14</sup>W. T. Doyle, *Phys. Rev. B* **39**, 9852 (1989).

<sup>15</sup>C. F. Bohren and D. R. Huffman, *Absorption and Scattering of Light by Small Particles* (John Wiley, New York, 1983).

<sup>16</sup>W. Rechberger, A. Hohenau, A. Leitner, J. Krenn, B. Lamprecht, and F. Aussenegg, *Opt. Commun.* **220**, 137 (2003).

<sup>17</sup>K. Su, Q. Wei, X. Zhang, J. Mock, D. Smith, and S. Schultz, *Nano Lett.* **3**, 1087 (2003).

<sup>18</sup>T. Atay, J.-H. Song, and A. V. Nurmikko, *Nano Lett.* **4**, 1627 (2004).

<sup>19</sup>J. B. Lassiter, J. Aizpurua, L. I. Hernandez, D. W. Brandl, I. Romero, S. Lal, J. H. Hafner, P. Nordlander, and N. J. Halas, *Nano Lett.* **8**, 1212 (2008).

<sup>20</sup>S. Marhaba, G. Bachelier, C. Bonnet, M. Broyer, E. Cottancin, N. Grillet, J. Lerme, J.-L. Vialle, and M. Pellarin, *J. Phys. Chem. C* **113**, 4349 (2009).

<sup>21</sup>V. A. Markel, *J. Mod. Opt.* **40**, 2281 (1993).

<sup>22</sup>V. V. Gozhenko, L. G. Grechko, and K. W. Whites, *Phys. Rev. B* **68**, 125422 (2003).

<sup>23</sup>A. Pinchuk and G. Schatz, *Nanotechnology* **16**, 2209 (2005).

<sup>24</sup>B. Khlebtsov, A. Melnikov, V. Zharov, and N. Khlebtsov, *Nanotechnology* **17**, 1437 (2006).

<sup>25</sup>J. D. Jackson, *Classical Electrodynamics*, 3rd ed. (John Wiley & Sons, New York, 1999), Chap. 9.

<sup>26</sup>J. J. Xiao, J. P. Huang, and K. W. Yu, *Phys. Rev. B* **71**, 045404 (2005).

<sup>27</sup>I. Romero, J. Aizpurua, G. W. Bryant, and F. J. G. D. Abajo, *Opt. Express* **14**, 9988 (2006).

<sup>28</sup>B. Stout, J. C. Auger, and A. Devilez, *J. Opt. Soc. Am. A* **25**, 2549 (2008).

<sup>29</sup>P. Olk, J. Renger, M. T. Wenzel, and L. M. Eng, *Nano Lett.* **8**, 1174 (2008).

<sup>30</sup>N. Bonod, A. Devilez, B. Rolly, S. Bidault, and B. Stout, *Phys. Rev. B* **82**, 115429 (2010).

<sup>31</sup>M. Abramowitz and I. A. Stegun, *Handbook of Mathematical Functions with Formulas, Graphs, and Mathematical Tables*, 9th Dover printing ed. (Dover, New York, 1964).

<sup>32</sup>B. Stout, J. Auger, and J. Lafait, *J. Mod. Opt.* **48**, 2105 (2001).